Environ Fluid Mech (2012) 12:63–80
DOI 10.1007/s10652-011-9214-3

ORIGINAL ARTICLE

Integrated modeling of flood flows and tidal hydrodynamics over a coastal floodplain

Zhaoqing Yang · Taiping Wang · Tarang Khangaonkar · Stephen Breithaupt

Received: 30 December 2010 / Accepted: 20 May 2011 / Published online: 2 July 2011

Abstract The interactions of physical processes between estuaries and upstream river floodplains are of great importance to the fish habitats and ecosystems in coastal regions. Traditionally, a hydraulic analysis of floodplains has used one- or two-dimensional models. While this approach may be sufficient for planning the engineering design for flood protection, it is inadequate when floodwaters inundate the floodplain in a complex manner. Similarly, typical estuarine and coastal modeling studies do not consider the effect of upstream river floodplains because of the technical challenge of modeling wetting and drying processes in floodplains and higher bottom elevations in the upstream river domain. While various multi-scale model frameworks have been proposed for modeling the coastal oceans, estuaries, and rivers with a combination of different models, this paper presents a modeling approach for simulating the hydrodynamics in the estuary and river floodplains, which provides a smooth transition between the two regimes using an unstructured-grid, coastal ocean model. This approach was applied to the Skagit River estuary and its upstream river floodplain of Puget Sound along the northwest coast of North America. The model was calibrated with observed data for water levels and velocities under low-flow and high-flood conditions. This study successfully demonstrated that a three-dimensional estuarine and coastal ocean model with an unstructured-grid framework and wetting-drying capability can be extended much further upstream to simulate the inundation processes and the dynamic interactions between the estuarine and river floodplain regimes.

Keywords Integrated modeling · Coastal floodplain · Estuary · Tide · Flood · Hydrodynamics

1 Introduction

Economic development, agricultural land use, and human activities in the coastal regions have altered the infrastructures and ecosystems from nearshore zones to upstream river floodplains.

Z. Yang (✉) · T. Wang · T. Khangaonkar · S. Breithaupt
Pacific Northwest National Laboratory, 1100 Dexter Avenue North, Suite 400, Seattle, WA 98109, USA
e-mail: zhaoqing.yang@pnnl.gov

The marine nearshore environment is the aquatic interface between freshwater, air, land, and marine waters, which provides a rich and important habitat for numerous aquatic organisms. The nearshore zone commonly includes areas from estuaries seaward that are influenced by marine waters and extends upstream in estuaries to the head of tidal influence. The marine nearshore habitat, which provides important buffer zones and links between terrestrial and marine ecosystems, is among the most productive ecosystems where biological processes, such as sunlight-driven photosynthesis, primary productivity, and carbon cycling occur [1–3].

The upstream river floodplain region is beyond the point of tidal influence and below the upland river reaches. Upstream river floodplains provide a significant off-channel habitat for a variety of salmon species during spawning, larva drift, and downstream migration periods in the Pacific Northwest [4,5]. Upstream off-channel habitat generally includes overflow channels, sloughs, wetlands, and small streams within the floodplains [6]. The periodic inundation of floodplain habitat enhances the lateral exchange of nutrients and water quality, which are important to juvenile fish survival. Floodplain habitat also provides shelter for juvenile fish from high velocities and predators. Flow regulations by hydropower dams and flood events during the high run-off season alter the natural connection of a river system to its floodplains. Hydro-modifications, such as constructing levees and armoring riverbanks as well as diverting water for agriculture along the river systems, also limit the usage of floodplain habitat by juvenile fish. Reconnection to the floodplain habitat is an important step in establishing and maintaining Pacific Northwest salmon populations [7–11].

Numerical models have been used to simulate the hydrodynamics and evaluate the restoration alternatives for improving habitats and connectivity in the nearshore and river floodplain regions as well as river stream and upstream floodplains [12–22]. A conventional hydrodynamic analysis for upstream floodplain is often conducted using one-dimensional (1D) models with the assumption that the lateral or vertical variations are small. The approach of 1D modeling in river floodplains may be sufficient for planning the engineering design of levees along the river channel for flood protection. However, it is inadequate when floodwaters flow across the floodplain in a complex manner, and lateral distributions of velocity magnitude, water depth, and inundation time and area become important for assessing floodplain habitat and managing fish migration and recovery. On the other hand, most of the hydrodynamic models developed for coastal and estuarine regions are in a three-dimensional (3D) domain because of high lateral variations and vertical stratifications. However, typical estuarine and coastal circulation modeling studies do not consider the effect of floodplains at the upstream river boundary because of either the challenge of model stability in simulating sloping river channels and the high computational demand or the assumption of negligible interactions between coastal zones and upstream floodplains.

Various multi-scale modeling frameworks have been developed by linking longitudinal 1D or laterally averaged two-dimensional (2D) river models with depth-averaged 2D or fully 3D estuarine coastal models [23–26]. However, this is insufficient to accurately characterize the physical processes, such as velocity magnitudes, water depths, and inundation time, in upstream floodplains using 1D or laterally averaged 2D models. Therefore, to properly model the interactions between river floodplains and estuarine zones and provide vital physical habitat information that is crucial to the nearshore and riparian ecosystems [1], it is important to simulate the hydrodynamics in estuarine regions and upstream floodplains in a single modeling domain using the same 3D model.

This paper presents a modeling approach to simulate the hydrodynamics in estuarine regions and upstream river floodplains using a 3D, unstructured-grid, coastal ocean model. This approach provides a smooth transition for model solutions between estuaries and river floodplains without the concern of numerical errors that might be introduced by linking

different models with different dimensions. The modeling approach was applied to simulate the hydrodynamics in the Skagit River estuary of Puget Sound and its upstream floodplain using the unstructured-grid Finite Volume Coastal Ocean Model (FVCOM) [27,28]. The model was validated with observed data for water levels and velocities under low-flow and high-flood conditions. This study demonstrated that an estuarine and coastal ocean model could be extended much further upstream to the river floodplain to simulate the inundation process and the dynamic interaction between the estuary and upstream floodplain regions. The structure of the paper is as follows. Section 2 provides a detailed description of the study domain. The methodology and model setup is given in Sect. 3, followed by model calibration results and discussion in Sect. 4. A summary of this study is given in Sect. 5.

2 Study domain—Skagit River estuary and middle Skagit River

The Skagit River originates in southwestern British Columbia in Canada and northwestern Washington in the United States. The river receives a number of tributaries over a length approximately 240 km, and the Skagit watershed drains an area of 8000 km^2 of the Cascade Range along the northern end of Puget Sound (Fig. 1). The largest tributary, the Sauk River, enters the Skagit River at 108 km (River Mile 67) from the Skagit River mouth. The Skagit River receives its second largest tributary, the Baker River, at 17 km downstream of the Sauk River. The Middle Skagit River, which is defined as the river reach between Sedro Woolley and the confluence of Sauk River and Upper Skagit River (Fig. 1), consists of a large area of floodplain that supports important and valuable fish habitats. The bottom elevation of the river channel at the upstream boundary is about 60 m higher than the mean water level in Skagit Bay. The Skagit River enters Skagit Bay through the North Fork and the South Fork branches, which were diked extensively for flood protection for agricultural land use.

The Skagit River is the largest river discharge to Puget Sound, responsible for about 34–50% of the total freshwater flow into Puget Sound. The river flow generally shows a two-peak distribution pattern in late spring or early summer because of snowmelt and in winter because of high precipitation. The river flow often drops to the minimum in September. A significant portion of Skagit Bay is covered by a shallow-water tide flat that becomes dry during low tides. Skagit Bay connects to Puget Sound and the Strait of Juan de Fuca (SJDF) through three pathways and is subjected to strong tidal forcings. The main pathway for water exchange with Puget Sound is the Saratoga Passage of Whidbey Basin from the south, which connects to the Main Basin of Puget Sound. Deception Pass connects Skagit Bay from the east to SJDF, and the Swinomish Channel connects Skagit Bay from the north to Padilla Bay, which in turn connects to SJDF.

The Skagit River estuary and its upstream river floodplain provide vital marine brackish water and freshwater habitats for Puget Sound Chinook, bull trout, and steelhead, which are all listed under the Endangered Species Act. To better protect these valuable species and fish habitats, it is important to understand the physical processes of the river system in both the estuarine environment and the upstream river floodplain. Previous research efforts studied salinity stratification and estuarine circulation in Skagit River estuary [29], the dynamics of tidal channel and delta in Skagit Bay [30], and thermal diffusivities in tide flat sediment [31].

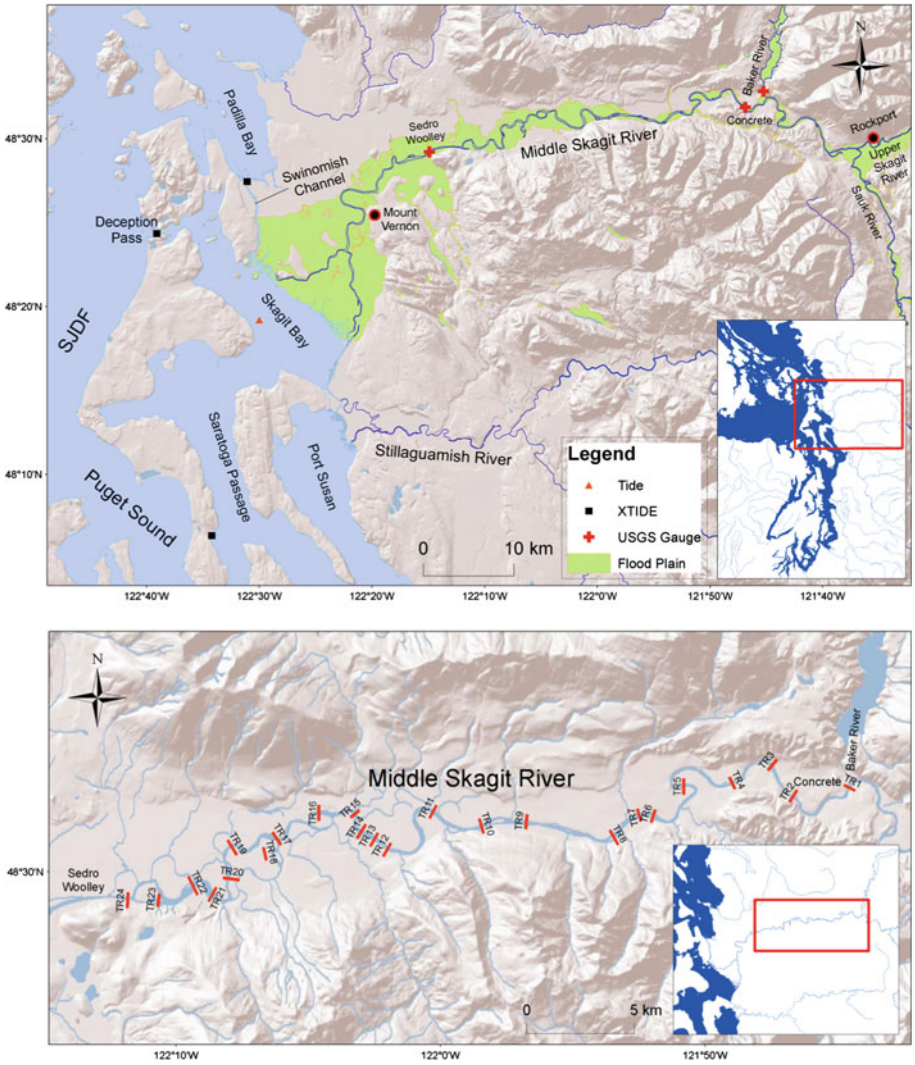

Fig. 1 Study domain—Skagit River Estuary and Middle Skagit Floodplain (*upper panel*) and observed velocity transects in the Middle Skagit River (*lower panel*)

3 Methodology

3.1 Data

Data used in this study can be divided into two groups: (1) data required for the model setup and (2) data used for the model calibration. Data required for the model setup consist of geometry and bathymetry data for the study domain and the boundary forcing data to drive the model. Model calibration data include observed values of physical properties to calibrate the model parameters and assess the model performance in simulating the hydrodynamics in the estuarine and upstream river floodplain regions.

Bathymetric data used to define the bottom elevation of the model grid were from several sources. Bathymetry data from the digital elevation model (DEM) of Puget Sound used to define the Skagit River estuary and bay areas in the model domain were at a horizontal resolution of 9 m by 9 m [32]. River cross-section survey data are generally limited. In this study, the river bathymetry data were obtained from river cross-sections of the U.S. Army Corps of Engineers' 1D HEC-RAS hydraulic model for the Skagit River [33]. The HEC-RAS river cross-sections were projected onto the Skagit River channel alignment and interpolated as the FVCOM model bathymetry in the Middle Skagit River channel. Another important portion of the bathymetry data required in this study is ground elevations in tide flats and the Middle Skagit River floodplain. The Light Detection And Ranging (LiDAR) bare-earth elevation data from the Puget Sound LiDAR Consortium (PSLC) were used to define the model bathymetry in the tide flats of Skagit Bay and near the mouth of the Skagit River estuary. The floodplain area in the model domain is defined based on the flood area identified in the Flood Warning Map issued by Skagit County [34]. LiDAR data collected by Skagit County were used to define elevations in the Middle Skagit River floodplain. All bathymetry data used in the model development were relative to the North American Vertical Datum of 1988 (NAVD88).

Model calibration data include water levels and velocities. Water level data at the U.S. Geological Survey (USGS) stream gages at Concrete and Sedro Woolley stations in the Middle Skagit River were obtained for model calibration during high-flood conditions from 10/05/2003 to 11/05/2003. Tidal elevation data in the Skagit Bay were used for model calibration under low-flow conditions from 11/17/2008 to 12/04/2008, with an average river inflow of 283 m^3/s, which was close to the long-term, monthly, mean low-flow rate of 266 m^3/s. Velocity data along 24 transect locations in the Middle Skagit River were collected by Puget Sound Energy during the periods of August 2002 and March 2003 with the Acoustic Doppler Current Profiler and the Price AA current meter (Fig. 1). Stage-discharge rating curves were developed for the transect locations on the Middle Skagit River using the measured data and velocity profiles that were estimated for three flow conditions: (1) low flow of 127.43 m^3/s, (2) medium flow of 311.5 m^3/s, and (3) high flow of 651.31 m^3/s.

3.2 Coastal ocean hydrodynamic model—FVCOM

There are many well developed and widely used 3D coastal ocean models available for simulating the hydrodynamics in estuarine and coastal environments and in fresh waters. Two important components in terms of model requirements in this study are the unstructured-grid model framework and the capability to simulate wetting and drying processes in both intertidal zones and upstream sloping floodplains. FVCOM is a 3D, unstructured-grid, coastal ocean model with the robust capability of simulating wetting and drying processes in the tide flat and floodplain [27]. A finite-volume approach is used in FVCOM that combines the advantages of finite-element methods for geometric flexibility and finite-difference methods for simple discrete structures and computational efficiency. Unstructured triangular cells are used in the horizontal plane and a sigma-stretched coordinate system is employed in the vertical direction to better represent the bottom topography.

FVCOM solves the 3D momentum, continuity, temperature, salinity, and density equations in an integral form for water surface elevation and flow fields. Companion modules for sediment transport, water quality kinetics, and biological models are also integrated into FVCOM. The model employs the Smagorinsky scheme for horizontal mixing [35] and the

Mellor Yamada, level 2.5, turbulent closure scheme for vertical mixing [36]. FVCOM has been widely used to simulate circulations in coastal and estuarine environments [29,37–42], storm surge predictions [43–45], and nearshore restorations [15,16].

The wetting and drying process in FVCOM is simulated using the point treatment technique based on following criterion [42], for any given node

$$\begin{cases} \text{wet}, & \text{if } D = h + \eta > D_{\min} \\ \text{dry}, & \text{if } D = h + \eta \leq D_{\min} \end{cases}$$

and for any given triangular cell

$$\begin{cases} \text{wet}, & \text{if } D = \min(h_{N1}, h_{N2}, h_{N3}) + \max(\eta_{N1}, \eta_{N2}, \eta_{N3}) > D_{\min} \\ \text{dry}, & \text{if } D = \min(h_{N1}, h_{N2}, h_{N3}) + \max(\eta_{N1}, \eta_{N2}, \eta_{N3}) \leq D_{\min} \end{cases}$$

where h and η are the bathymetric height and water surface elevation related to the referenced datum (NAVD88) in the model, respectively; $N1$, $N2$, $N3$ are the three node numbers of a triangular cell; $D_{\min}$ is the minimum depth criterion for wetting and drying simulation. When a triangular cell is treated as dry, the cell velocity and fluxes across the three sides of the cell are set to zero.

3.3 Model setup for Skagit Bay and middle Skagit Floodplain

An unstructured-grid for Skagit Bay and the Middle Skagit River floodplain was developed using the Puget Sound digital elevation model, the HEC-RAS model river cross-sections of the Skagit River, and LiDAR data as described in Sect. 3.1. The model grid consists of roughly 45,000 triangular cells and 25,000 nodes in the horizontal plane. Ten uniform vertical sigma layers were specified in the water column. The resolution of the model grid ranges from 10 to 50 m in the river floodplain and around 20–100 m in Skagit Bay. The model grid was set up in Universal Transverse Mercator North American Datum 83 (UTM Zone 10, NAD83) in the horizontal plane, with reference to NAVD 88 in the vertical direction. Examples of model grids and bathymetries in Skagit Bay and a section of the Middle Skagit River floodplain are shown in Fig. 2.

Tidal elevations were specified using XTide predictions along three open boundaries in Saratoga Passage, Deception Pass, and the Swinomish Channel. Salinity open boundary conditions were approximated with constant values through the water column based on observations. Model upstream inflow boundary conditions were specified using stream-flow data from the USGS stream gages at the Concrete and Baker River stations at hourly intervals. Because the Concrete station includes all the flows from impounded reaches of the Upper Skagit and Baker Rivers as well as from the Sauk River, the river inflow at the upstream model boundary was calculated by subtracting the Baker River flow rate from the Concrete station flow. The Baker River was considered as a tributary discharge to the Skagit River in the model. River inflows for the high flow conditions in 2003 and the low-flow conditions in 2008 are shown in Fig. 3.

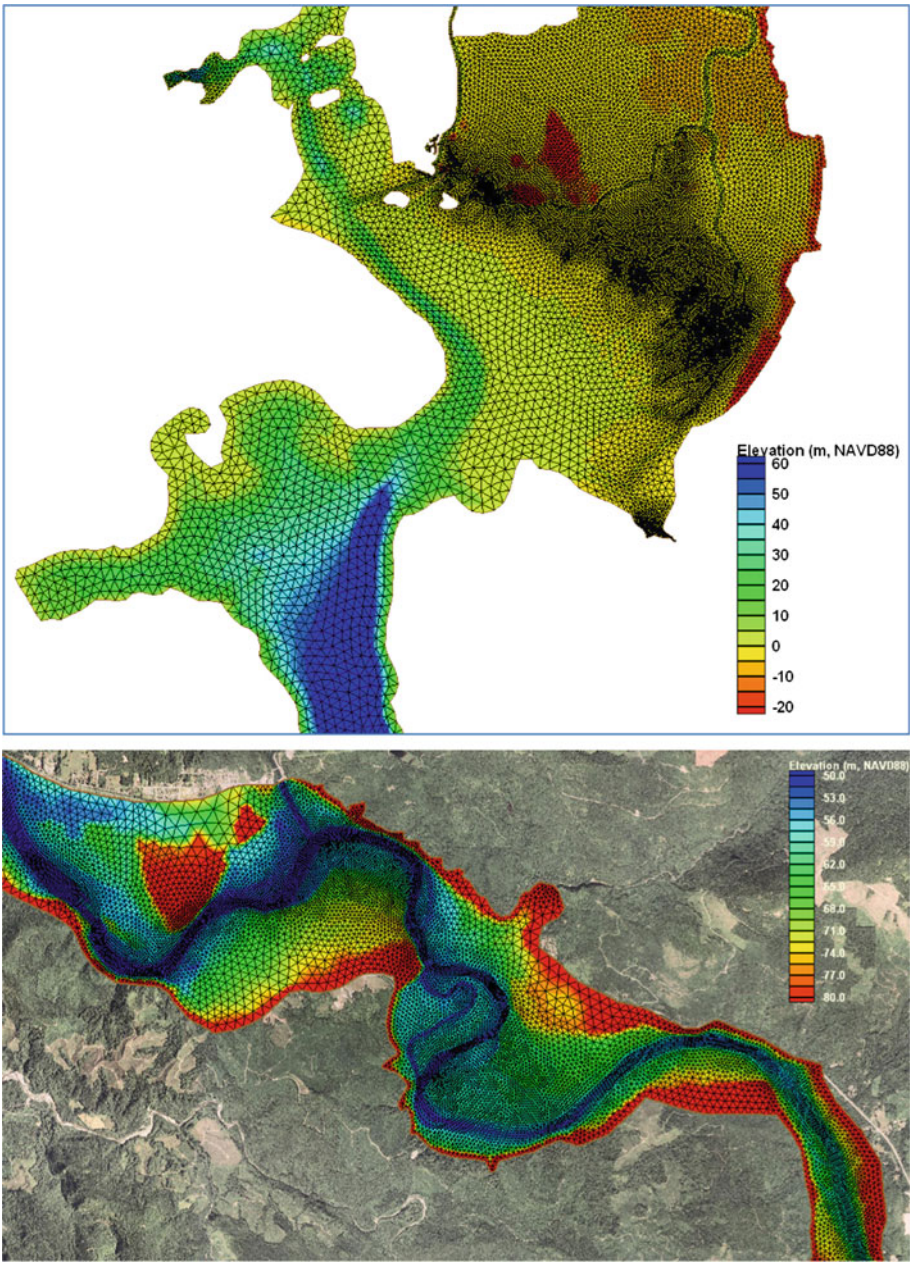

Fig. 2 Model grids and water depths in Skagit Bay (*upper panel*) and upstream reach of Middle Skagit River (*lower panel*)

The focus of this study is to demonstrate a coastal modeling capability to simulate the hydrodynamics in both estuarine and river floodplain regimes in an integrated modeling framework. Therefore, meteorological forcings (wind, heat flux, precipitation, and evaporation) and temperature simulations were not considered in this study.

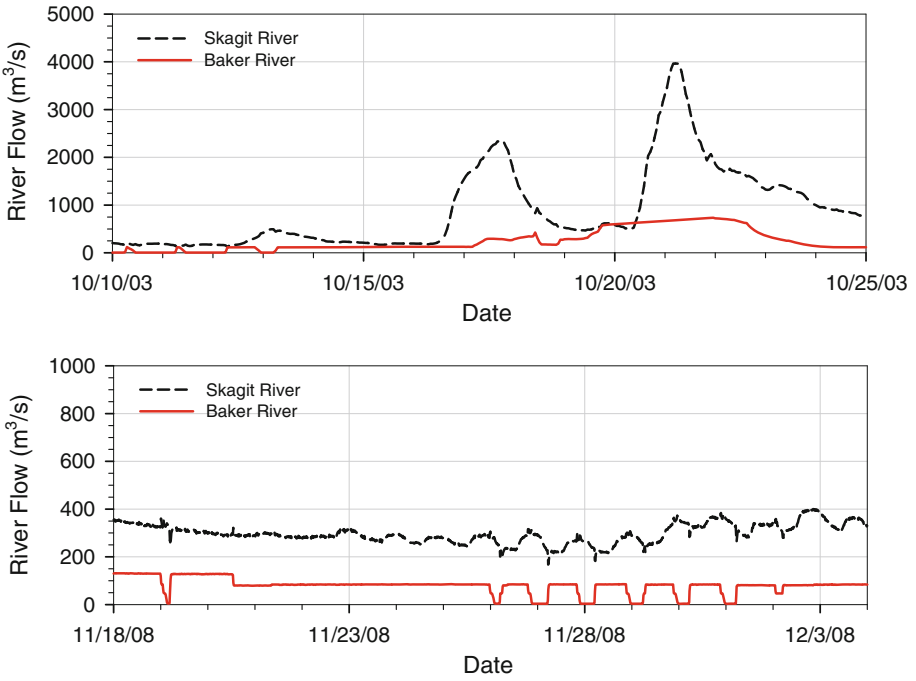

Fig. 3 Inflows of Skagit River and Baker River for the periods of 10/10/2003–10/25/2003 during flood events (*upper panel*) and 11/18/2008–12/4/2008 under low-flow conditions (*lower panel*)

4 Model calibration and result discussion

4.1 Model calibration for water levels and velocities

In this study, model calibration of the Skagit Bay and Middle Skagit River floodplain system was conducted with the focus on the Middle Skagit River floodplain using water-level data under flooding conditions and velocity data corresponding to three different flow regimes. A model external time step of 0.5 s was used, and an internal mode and external mode ratio of 5 was applied to maintain model stability under high-flood condition and complex inundation processes in the floodplain. A one-month long (31 days) model run took about 12 h to complete in parallel mode with 72 processors. A quadratic form of bottom friction is employed in the model. A spatially uniform bottom friction coefficient of 0.005 and a bottom roughness of 0.002 m were specified in the model. The linear Smagorinsky multiplicative coefficient was set to 0.2, and a background value of vertical eddy viscosity of 10^{-6} m^2/s was used. A minimum depth of $D_{\min} = 0.05$m was specified as the criterion for the wetting-drying simulation in the model. A typical model calibration with a 1D or 2D simulation of river hydraulics is conducted by adjusting the Manning' bed roughness coefficient, which is similar to the bottom roughness coefficient in the 3D coastal ocean model. However, the main challenge of model calibration in an estuary and river floodplain system under flooding conditions is to properly include the off-channel water storage in the floodplain. Therefore, an accurate representation of floodplain elevations and side channels becomes the most important factor in model calibration for water levels in this study. Initial model results indicated that the model

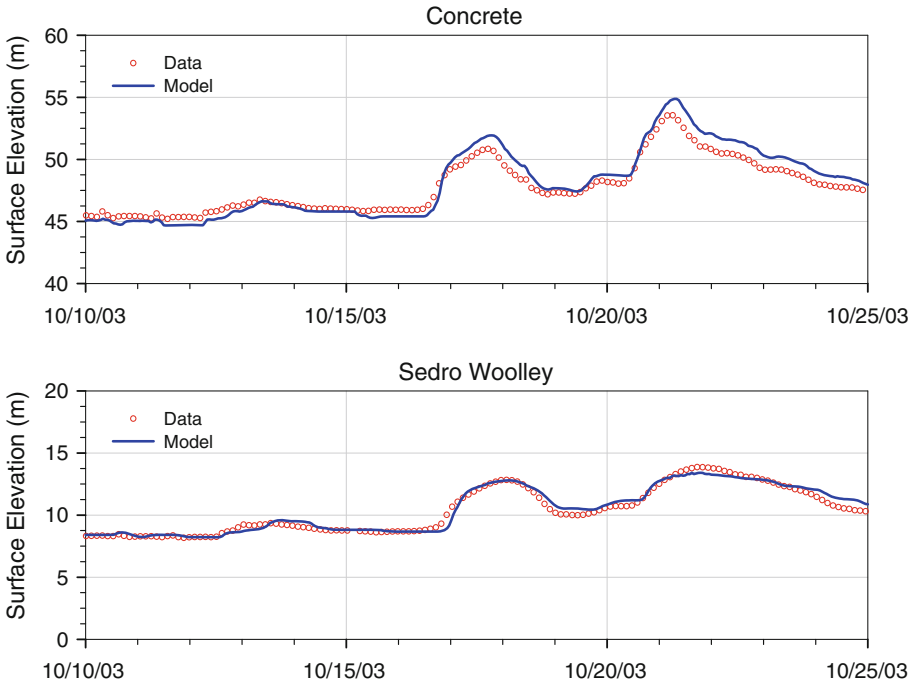

Fig. 4 Comparisons of modeled and observed water-surface elevations at Concrete and Sedro Woolley gauges under high-flood conditions

over-predicted water levels in the river without proper inclusion of off-channel floodplain under flood conditions. Compared with ground-truth spot measurements of ground elevations in the Middle Skagit River floodplain, it was found that LiDAR data were higher than the surveyed elevations in densely vegetated locations in the floodplain. Similarly, LiDAR data also showed higher bottom elevations in some shallow tidal channels and ponding water areas in the Skagit Bay front. Thus, model bathymetry in the floodplain was adjusted in those areas where LiDAR data were affected by dense vegetation and ponding water areas based on available ground survey data.

Comparisons of simulated and observed water levels at Concrete and Sedro Woolley stations are shown in Fig. 4. Model predictions matched the general distribution patterns of water levels at both stations and reproduced the two peaks in water level that correspond to the two high-flood events. Water levels increased about 9 and 5 m, respectively, at Concrete and Sedro Woolley during the 10/21/2003 high-flood event. The model prediction at Sedro Woolley station shows better agreement with data than that at the Concrete station. At the Concrete station, the model tended to slightly underpredict the water level during low-flow conditions when no overtopping occurred along the riverbanks and over-predicted the water level during the high-flood event. This discrepancy could be caused by the fact that the Concrete station is too close to the upstream river boundary where inflow boundary conditions were employed.

A detailed study of hydrodynamics and model calibration for the Skagit River estuary was conducted previously by Yang and Khangaonkar [29]. To validate the model performance of tidal simulation with the extension to the Middle Skagit River floodplain, a model simulation

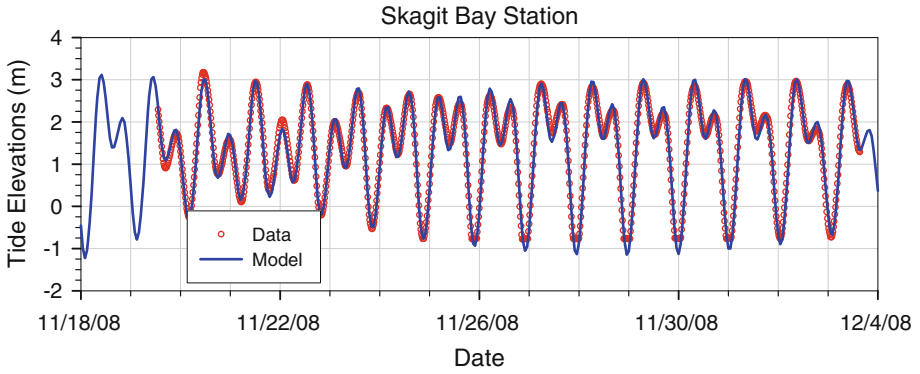

Fig. 5 Comparison of modeled and observed water surface elevations at Skagit Bay under low-flow conditions

was conducted and compared to observed tidal elevation data for the period of 11/17/2008–12/4/2008 under low-river-flow conditions. Figure 5 indicated that predicted tidal elevations matched the observed data well in Skagit Bay. Tides in Skagit Bay are mixed, semi-diurnal dominant tides and show large inequalities in tidal ranges and the strong spring-neap tidal cycle.

Predicted velocities in the Middle Skagit River reach were also compared to observed velocity data for three controlled river flow conditions. To simplify velocity calibration, cross-sectional average velocities were calculated along all transects and used for model calibration. Model simulations were conducted by specifying constant flows at the upstream river boundary that corresponded to the three controlled river flows during velocity observations (127.4, 311.5, and 651.3 m^3/s). Similar to the model calibration of water levels in the Middle Skagit River, velocity calibration was conducted primarily through grid refinement to better represent river channels with reference to LiDAR images and high-resolution aerial images. Comparisons of predicted and observed cross-sectional velocities along 24 transects in the Middle Skagit River are shown in Fig. 6. Overall, model predictions matched the observations well throughout the entire Middle Skagit River reach. Both model results and observed data showed consistent distribution patterns of cross-sectional average velocities for all three flow conditions. Figure 6 also indicated that at most of the transects, velocities increased linearly as the river flow increased because water was confined within the river channel under all three flow conditions.

4.2 Model skill assessment

To quantitatively measure the accuracy of model calibration, a model skill assessment for the model calibration was conducted based on the following error statistics:

- Mean error: $ME = \frac{1}{N}\sum_{i=1}^{N}\left(\eta_i^m - \eta_i^o\right)$, where N is the total data points of field observations, η_i^m is model prediction, and η_i^o is observation.
- Mean absolute error: $MAE = \frac{1}{N}\sum_{i=1}^{N}\left|\eta_i^m - \eta_i^o\right|$
- Root mean square error: $RMSE = \sqrt{\frac{1}{N}\sum_{i=1}^{N}\left(\eta_i^m - \eta_i^o\right)^2}$
- Relative error: $RE = 100\% \times \frac{\sum_{i=1}^{N}\left(\eta_i^m - \eta_i^o\right)^2}{\sum_{i=1}^{N}\left|\eta_i^o\right|}$

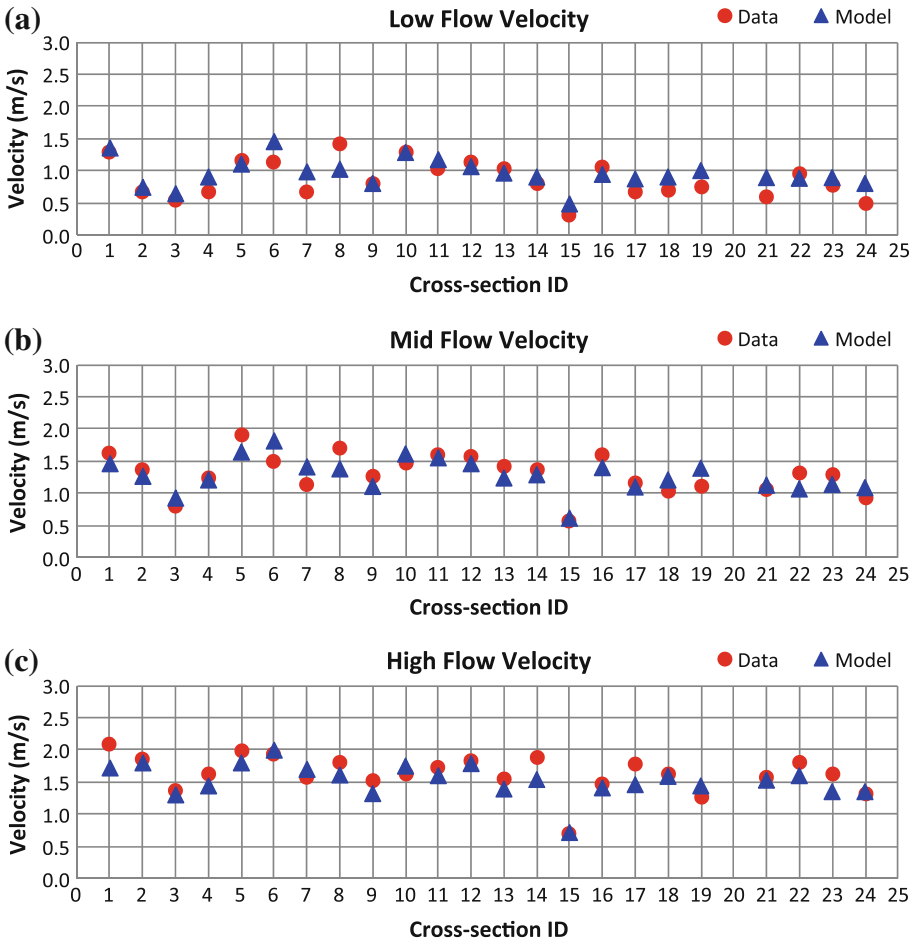

Fig. 6 Comparisons of modeled and observed cross-sectional average velocities in upstream Skagit floodplain during **a** low-flow, **b** medium-flow, and **c** high-flow conditions

Error statistics for model calibration of water levels and cross-sectional velocities are provided in Tables 1 and 2, respectively. Table 1 shows that relative errors for water-level calibration for all three stations were below 5%. The model shows the most accurate results in terms of simulating tidal elevations at the Skagit Bay station with 0.12 m root mean square error (RMSE) and 0.6% relative error (RE). Although the RMSE for the water-level calibration at the Concrete station is 0.76 m, the RE is still small (1.8%) due to a large variation of water levels during the high-flood event. To analyze the overall accuracy of velocity calibration, average error statistics for all the velocity transects were calcualted. Table 2 shows that the velocity prediction errors for three flow conditions were similar. All RMSEs were within the reasonable range of 0.2 m/s, and REs were under 20%.

4.3 Model results discussion

Figure 7 shows the snapshots of water depth and velocity distributions in the Middle Skagit River floodplain under low-flow, medium, and high-flood conditions. During low-flow

Table 1 Error statistics for water-surface-elevation calibration

Station	ME (m)	MAE (m)	RMSE (m)	RE (%)
Concrete Gauge	0.28	0.66	0.76	1.4
Sedro Woolley Gauge	0.09	0.26	0.34	2.5
Skagit Bay	−0.03	0.10	0.12	0.6

Table 2 Error statistics for velocity calibration

Station	ME (m/s)	MAE (m/s)	RMSE (m/s)	RE (%)
Low flow	0.09	0.16	0.20	18.7
Medium flow	−0.03	0.16	0.18	12.6
High flow	0.10	0.15	0.18	9.0

conditions (on 11/29/2008 when river inflow was below 300 m^3/s), water flowed within the river channel, and no overtopping of river banks occurred (Fig. 7a). During medium-flood conditions (on 10/17/2003 when river inflow was about 2000 m^3/s), water started to overtop the river bank and inundate the floodplain through side channels (Fig. 7b). During high-flood conditions (on 10/21/2003 when river inflow peaked at nearly 4000 m^3/s), almost the entire floodplain was inundated (Fig. 7c), though the strongest velocities remained in the main river channel.

Velocity and salinity distributions during low-flow and high-flood conditions were also examined in the lower Skagit River delta and Skagit Bay. Figure 8 shows the surface velocity and salinity distributions during flood and ebb tides under low-flow and high-flood conditions. Under low-flow conditions (11/29/2008), a strong salinity intrusion occurred in the tide flat region of Skagit Bay during flood tide (Fig. 8a) while the tide flat region started to dry during ebb tide. Most of Skagit Bay was occupied by brackish water (Fig. 8b). The lower Skagit River floodplain and delta remained dry under low river flow conditions. A siginificant portion of the lower river floodplain and delta was inundated under high-flood conditions (10/21/2003) (Fig. 8c, d). In particular, a greater area was inundated during flood tide (Fig. 8c) than ebb tide (Fig. 8d), and salinity in the bay front and tide flat region dropped significantly down to a single digit throughout the entire tidal cycle under high-flood conditions.

Figure 9 shows a vertical transect (see Fig. 1) of daily average salinity and velocity distributions from Saratoga Passage to Skagit Bay and further up to the upstream river boundary under low-flow and high-flood conditions. Clearly, the water level at the upstream river floodplain was significantly higher (about 55 m) than the water level in the Skagit Bay (Fig. 9a, c). Salinity stratification in Skagit Bay was present even during low-flow conditions because the Skagit River is the largest river discharging into Puget Sound (Fig. 9a). During high-flood conditions, the water level was elevated in the Middle Skagit River reach (Fig. 9c) compared to low-flow conditions (Fig. 9a). Salinity stratification was significantly enhanced with a surface salinty less than 10 ppt in Skagit Bay, and the salt intrusion point was pushed more than 2.0 km downstream under high-flood conditions (Fig. 9c). Mean velocities of longitudinal daily averages are shown in Fig. 9 (b, d). In both low-flow and high-flood conditions, mean currents in the North Fork branch of the Skagit River were always towards the downstream direction (negative values). Vertical two-layer estuarine circulations were clearly seen in both low-flow and high-flood conditions, but were much enhanced during the high-flood event.

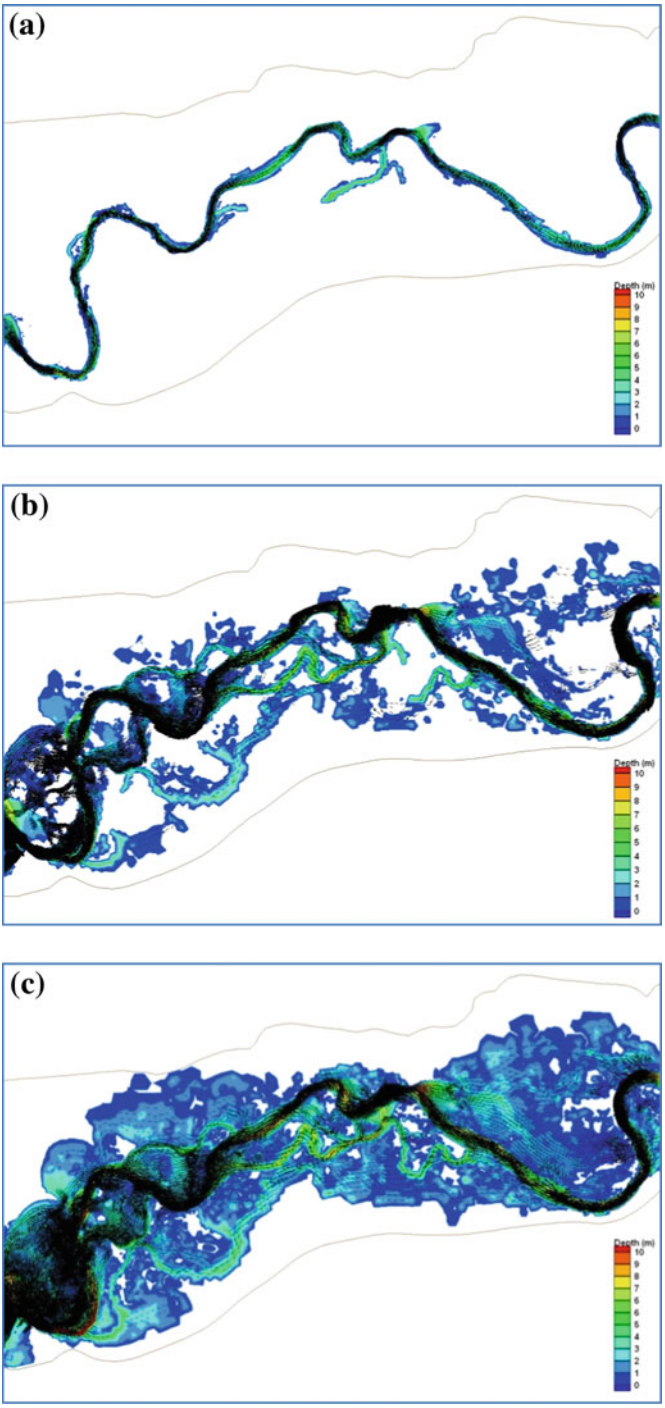

Fig. 7 Water-depth and surface-velocity distributions in the Middle Skagit Reach under **a** low-flow (11/29/2008), **b** medium-flood (10/17/2003), and **c** high-flood (10/21/2003) conditions. The *white-color* region inside the model domain indicates dry areas

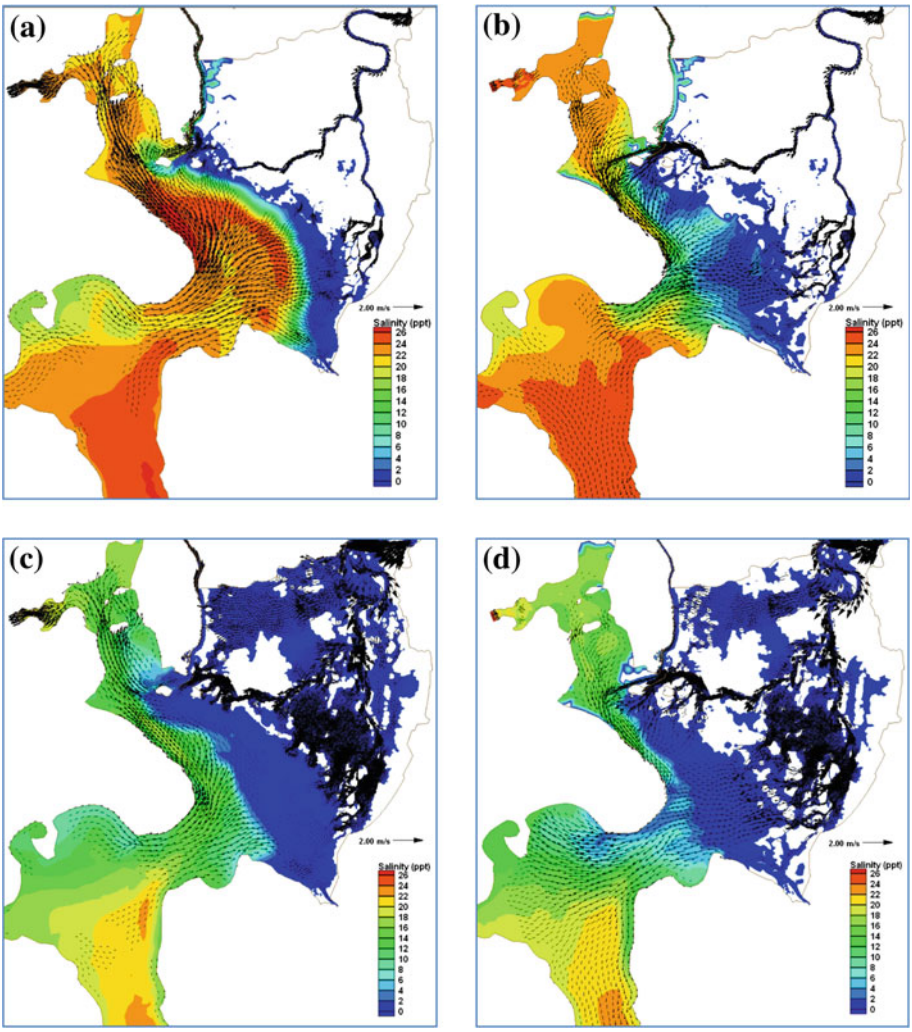

Fig. 8 Surface salinity and velocity distributions in Skagit Bay under low-flow conditions (11/29/2008) during flood tide (**a**) and ebb tide (**b**) and under high-flood conditions (10/21/2003) during flood tide (**c**) and ebb tide (**d**). The *white-color* region inside the model domain indicates dry areas

5 Summary

In this study, a modeling approach to integrate the simulations of hydrodynamics in an estuary and upstream river floodplain system using a 3D, unstructured-grid, coastal ocean model is presented. Unlike other modeling approaches, which often externally link the 3D estuarine and coastal models to 1D or 2D river models, this modeling approach provides continuous simulations of physical processes in estuarine and coastal waters and elevated upstream floodplains as well as the interactions between these two regimes. A model application to the Skagit Bay and Middle Skagit River floodplain system demonstrated that an unstructured-grid, coastal ocean model with a wetting and drying capability can be used to simulate

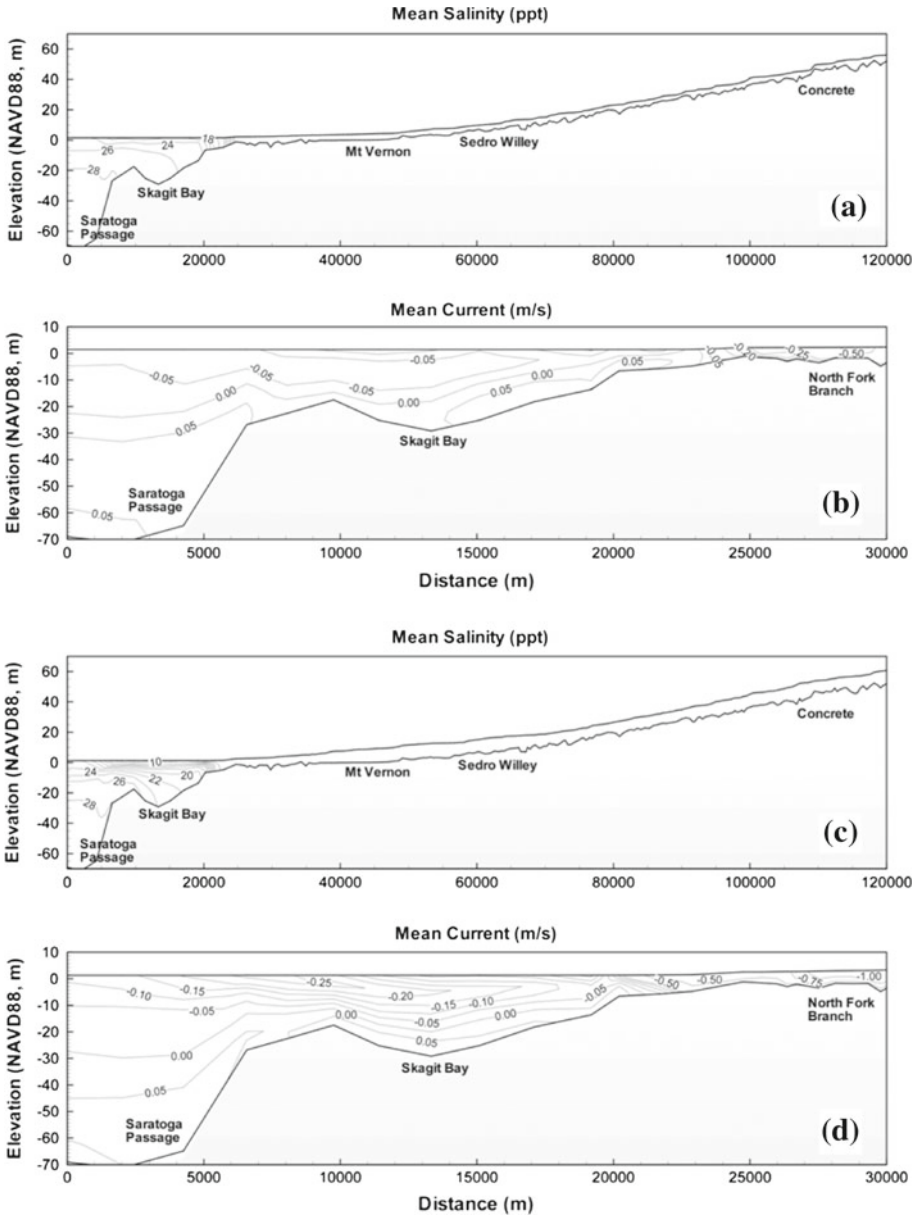

Fig. 9 Vertical profiles of daily average salinity and current distributions from Skagit Bay to upstream boundary under low-flow (**a**, **b**) and high-flood conditions (**c**, **d**). Negative current values indicate outgoing flow direction

the 3D hydrodynamics in the nearshore and floodplain regimes and provide crucial habitat parameters, such as inundation frequency and duration, flooding areas, velocity, water depth, and salinity distributions.

Applying the model to the Skagit Bay and Middle Skagit River floodplain system indicated that three key elements are essential for successfully modeling an estuary and upstream flood-

plain system. First is the unstructured-grid modeling framework that provides the flexibility of simulating complex features, such as tide flats and floodplain geometry, multiple tidal channels and off-main-stem side channels, as well as infrastructures (e.g., levees). The second key element is a robust model scheme to stably simulate the wetting and drying processes, not only in the tide flat region, but also in the high-elevated, upstream floodplains. Finally, to simulate the water-storage in the floodplain properly, high-resolution LiDAR elevation data combined with ground-truth measurements are necessary to better define the model bathymetry in the tide flat and upstream river floodplain regions.

While this paper presents promising results for integrating the modeling of hydrodynamics in an estuarine and floodplain system, many challenging issues remain for future study. For example, model validation was not conducted in the floodplains because of no measured data. To ensure accurate simulation of inundation process in the floodplains, model validation in the floodplains should be considered in future study with various data sources and methods [46,47]. Wind effects on circulation and wind-induced storm surges were not considered in this study. The interactions of wind-induced storm surges with river flood and extreme tides could result in significant increases of water levels. Properly estimating the net heat flux exchange and accurately simulating temperature dissipation in tide flats and upstream floodplains is still a challenging research topic. Furthermore, the bottom roughness plays an important role in wetting and drying processes in tide flats and upstream floodplains. The employment of spatially varying bottom roughness based on vegetation and sediment information may be necessary to improve model prediction of water inundation in tide flats and upstream floodplains.

Acknowledgements This model development was conducted through partial funding from the Skagit Watershed Council (SWC) and the Skagit River System Corporative (SRSC) as part of the Middle Skagit River and the Gilligan Creek Restoration Projects, as well as an EPA-STAR grant on Nonlinear Responses to Global Change in Linked Aquatic and Terrestrial Ecosystems (EPA-G2005-STAR-L1). Guidance and direction provided by Ms. Mary Raines of SWC and Mr. Devin Smith and Mr. Steve Hinton of SRSC are highly appreciated. We would also like to acknowledge Mr. Ed Connor of Seattle City Light who was the sponsor and provided velocity data for model calibration in the Middle Skagit River.

References

1. Day JW Jr, Hall CAS, Kemp WM, Yáez-Arancibia A (1989) Estuarine ecology. Wiley, Hoboken
2. Rupp-Armstrong S, Nicholls RJ (2007) Coastal and estuarine retreat: a comparison of the application of managed realignment in England and Germany. J Coastal Res 23(6):1418–1430
3. Schindler DE, Scheuerell MD, Moore JW, Gende SM, Francis TB, Palen WJ (2003) Pacific salmon and the ecology of coastal ecosystems. Frontiers Ecol Env 1(1):31–37
4. Beechie T, Beamer E, Wasserman L (1994) Estimating coho salmon rearing habitat and smolt production losses in a large river basin, and implications for habitat restoration. North Am J Fish Manag 14:797–811
5. Beamer E, Beechie T, Perkowski B, Klochak J (1999) Application of the Skagit watershed council strategy. Skagit Watershed Council, Mount Vernon
6. Smith D (2005) Off-channel habitat inventory and assessment for the upper Skagit River basin. Report to non-flow coordinating committee of the Skagit River hydroelectric project (FERC No. 553) by Skagit River System Cooperative, La Conner, WA
7. Phillips JL, Ory J, Talbot A (2000) Anadromous salmonid recovery in the Umatilla River Basin, Oregon: a case study. J Am Water Resour Assoc 36(6):1287–1308
8. Hanrahan TP, Dennis D, Dauble DD, Geist DR (2004) An estimate of Chinook Salmon (*Oncorhynchus tshawytscha*) spawning habitat and redd capacity upstream of a migration barrier in the upper Columbia River. Can J Fish Aquat Sci 61(1):23–33
9. Goodwin CN, Hawkins CP, Kershner JL (1997) Riparian restoration in the western United States: overview and perspective. Restor Ecol 5((4) (Supplement)):4–14

10. Karle KF, Densmore RV (1994) Stream and riparian floodplain restoration in a riparian ecosystem disturbed by placer mining. Ecol Eng 3:121–133
11. Palmer MA et al (2005) Standards for ecologically successful river restoration. J Appl Ecol 42:208–217
12. Hsu MH, Kuo AY, Kuo J-T, Liu W-C (1998) Modeling estuarine hydrodynamics and salinity for wetland restoration. J Environ Sci Health A 33(5):891–921
13. Brennan ML, May CL, Danmeier DG, Crooks S, Haltiner JH (2008) Numerical modeling of restoration alternatives in an erosional estuary. In: Spaulding ML (ed) Proceedings of the 10th international conference. American Society of Civil Engineers, Newport, RI, pp 942–960
14. Tsihrintzis VA, John DL, Tremblay PJ (1998) Hydrodynamic modeling of wetlands for flood detention. Water Resour Manag 12: 251–269. doi:10.1023/A:1008031011773
15. Yang Z, Khangaonkar T, Calvi M, Nelson K (2010) Simulation of cumulative effects of nearshore restoration projects on estuarine hydrodynamics. Ecol Model 221:969–977. doi:10.1016/j.ecolmodel.2008.12.006
16. Yang Z, Sobocinski KL, Heatwole D, Khangaonkar T, Thom R, Fuller R (2010) Hydrodynamic and ecological assessment of nearshore restoration: a modeling study. Ecol Model 221: 1043–1053. doi:10.1016/j.ecolmodel.2009.07.011
17. Callaghan DP, Bouma TJ, Klaassen P, Wal Dvan der , Stive MJF, Herman PMJ (2010) Hydrodynamic forcing on salt-marsh development: distinguishing the relative importance of waves and tidal flows. Estuar Coast Shelf Sci 89:73–88
18. Nestler JM, Milhous RT, Layzer JB (1989) Instream habitat modeling techniques. In: Gore JA, Petts G (eds) EAlternatives in regulative river management. CRC Press, Boca Raton, pp 295–315
19. Hostetler SW (1991) Analysis and modeling of long-term stream temperatures on the steamboat Creek Basin, Oregon: implications for land use and fish habitat. Water Res Bull WARBAQ 27(4):637–647
20. Scruton DA, Heggenes J, Valentin S, Harby A, Bakken TH (1998) Field sampling design and spatial scale in habitat-hydraulic modelling: comparison of three models. Fish Manag Ecol 5:225–240
21. Lamouroux N, Capra H, Pouilly M (1998) Predicting habitat suitability for lotic fish: Linking statistical hydraulic models with multivariate habitat use models. Reg Rivers: Res Manag 14:1–11
22. Bohn BA, Kershner JL (2002) Establishing aquatic restoration priorities using a watershed approach. J Environ Manag 64:355–363
23. Zang Y, Street RL (1995) A composite multigrid method for calculating unsteady incompressible flows in geometrically complex domains. Int J Numer Methods Fluids 20(5):341–361
24. Formaggia L, Gerbeau JF, Nobile F, Quarteroni A (2001) On the coupling of 3D and 1D Navier–Stokes equations for flow problems in compliant vessels. Comput Methods Appl Mech Eng 191(6–7):561–582
25. Chen X (2007) Dynamic coupling of a three-dimensional hydrodynamic model with a laterally averaged, two-dimensional hydrodynamic model. J Geophys Res 112:C07022. doi:10.1029/2006JC003805
26. de Brye B, de Brauwere A, Gourgue O, Kärnä T, Lambrechts J, Comblen R, Deleersnijder E (2010) A finite-element, multi-scale model of the Scheldt tributaries, river, estuary and ROFI. J Coastal Eng 57:850–863
27. Chen C, Liu H, Beardsley RC (2003) An unstructured, finite-volume, three-dimensional, primitive equation ocean model: application to coastal ocean and estuaries. J Atmos Ocean Tech 20:159–186
28. Chen C, Beardsley RC, Cowles G (2006) An unstructured grid, finite-volume coastal ocean model (FVCOM) system. Special issue entitled "advance in computational oceanography". Oceanography 19(1):78–89
29. Yang Z, Khangaonkar T (2009) Modeling tidal circulation and stratification in Skagit River estuary using an unstructured grid ocean model. Ocean Model 28:34–49. doi:10.1016/j.ocemod.2008.07.004
30. Hood WG (2010) Delta distributary dynamics in the Skagit River Delta (Washington, USA): extending, testing, and applying avulsion theory in a tidal system. Geomorphology. doi:10.1016/j.geomorph.2010.07.007
31. Thomson J (2010) Observations of thermal diffusivity and a relation to the porosity of tidal flat sediments. J Geophys Res 115:C05016. doi:10.1029/2009JC005968
32. Finlayson DP (2005) Combined bathymetry and topography of the puget lowland, Washington State. University of Washington. http://www.ocean.washington.edu/data/pugetsound/
33. U.S. Army Corps of Engineers (USACE) (2004) Draft report, Skagit River flood damage reduction study. Hydraulic technical documentation, Seattle, Washington
34. Skagit County Public Works (1996) Flood warning map for the Skagit River valley from Nookachamps area to Rockport area. Mt Vernon, Washington. ftp://ftp.skagitcounty.net/GIS/Documents/Flood/fld-warn.pdf Accessed 29 Dec 2010
35. Smagorinsky J (1963) General circulation experiments with the primitive equations. I. The basic experiment. Mon Weather Rev 91:99–164

36. Mellor GL, Yamada T (1982) Development of a turbulence closure model for geophysical fluid problems. Rev Geophys Space Phys 20:851–875
37. Chen C, Gao G, Qi J, Proshutinsky A, Beardsley RC, Kowalik Z, Lin H, Cowles G (2009) A new high-resolution unstructured-grid finite-volume Arctic Ocean model (AO-FVCOM): an application for tidal studies. J Geophys Res. doi:10.1029/2008jc004941
38. Xue P, Chen C, Ding P, Beardsley RC, Lin H, Ge J, Kong Y (2009) Saltwater intrusion into the Changjiang River: a model-guided mechanism study. J Geophys Res 114:C02006. doi:10.1029/2008JC004831
39. Li C, Chen C, Guadagnoli G, Georgiou IY (2008) Geometry induced residual eddies in estuaries with curved channel-observations and modeling studies. J Geophys Res 113:C01005. doi:10.1029/2006JC004031
40. Huang H, Chen C, Blanton JO, Andrade FA (2008) Numerical study of tidal asymmetry in the Okatee Creek, South Carolina, estuaries. Coast Shelf Sci 78:190–202
41. Yang Z, Khangaonkar T (2010) Multi-scale modeling of puget sound using an unstructured-grid coastal ocean model: from tide flats to estuaries and coastal waters. J Ocean Dynam 60: 1621–1637. doi:10.1007/s10236-010-0348-5
42. Chen C, Qi J, Li C, Beardsley RC, Lin H, Walker R, Gates K (2008) Complexity of the flooding/drying process in an estuarine tidal-creek salt-marsh system: an application of FVCOM. J Geophys Res 113:C07052. doi:10.1029/2007jc004328
43. Weisberg RH, Zheng L (2006) Hurricane storm surge simulations for Tampa Bay. Estuaries Coasts 29(6A):899–913
44. Qi J, Chen C, Beardsley RC, Perrie W, Cowles G (2009) An unstructured-grid finite-volume surface wave model (FVCOM-SWAVE): implementation, validations and applications. Ocean Model 28: 153–166. doi:10.1016/j.ocemod.2009.01.007
45. Huang Y, Weisberg RH, Zheng L (2010) Coupling of surge and waves for an Ivan-like hurricane impacting the Tampa Bay, Florida region. J Geophys Res 115:C12009. doi:10.1029/2009JC006090
46. Pappenberger F, Beven K, Frodsham K, Romanowicz R, Matgen P (2007) Grasping the unavoidable subjectivity in calibration of flood inundation models: a vulnerability weighted approach. J Hydrol 233: 275–287
47. Mason DC, Bates PD, Dall' Amico JT (2009) Calibration of uncertain flood inundation models using remotely sensed water levels. J Hydrol 233:275–287